

Changes of the transitional climate zone in East Asia: past and future

Lin Wang, Wen Chen, Gang Huang & Gang Zeng

Climate Dynamics

Observational, Theoretical and
Computational Research on the Climate
System

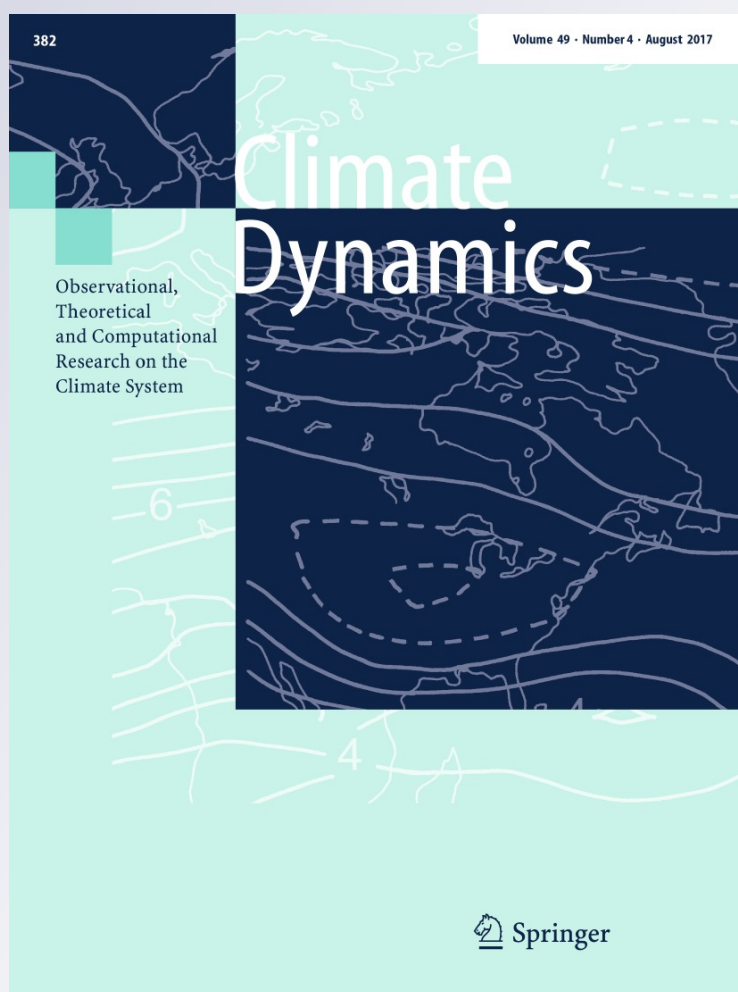
ISSN 0930-7575

Volume 49

Number 4


Clim Dyn (2017) 49:1463-1477

DOI 10.1007/s00382-016-3400-4



Your article is protected by copyright and all rights are held exclusively by Springer-Verlag Berlin Heidelberg. This e-offprint is for personal use only and shall not be self-archived in electronic repositories. If you wish to self-archive your article, please use the accepted manuscript version for posting on your own website. You may further deposit the accepted manuscript version in any repository, provided it is only made publicly available 12 months after official publication or later and provided acknowledgement is given to the original source of publication and a link is inserted to the published article on Springer's website. The link must be accompanied by the following text: "The final publication is available at link.springer.com".

Changes of the transitional climate zone in East Asia: past and future

Lin Wang^{1,2}  · Wen Chen^{3,4} · Gang Huang^{4,5} · Gang Zeng²

Received: 1 May 2016 / Accepted: 11 October 2016 / Published online: 17 October 2016
© Springer-Verlag Berlin Heidelberg 2016

Abstract The transitional climate zone (TCZ) between humid and arid regions in East Asia is characterized by sharp climate and biome gradients, interaction between the East Asian summer monsoon and the mid-latitude westerly winds and mixed agriculture-pasture activities. Consequently, it is highly vulnerable to natural disturbances and particularly human-driven global change. This study aims to illuminate the spatial and temporal variation of TCZ across both the retrospective and the prospective periods. In the historical period, both the front and rear edges of TCZ exhibit wide year-to-year excursions and have experienced coastward migration with increasing aridity throughout TCZ. Furthermore, precipitation fluctuation mainly contributes to interannual variability of TCZ whereas potential

evaporation behavior dominates the long-term trends of TCZ. Models are capable of largely reproducing the shape and orientation of TCZ, although northwestward bias is apparent. In global warming scenario period, there will be continuing southeastward displacement for the front edge but the opposite northwestward movement is projected for the rear one, as a consequence of significant drying trends in the humid zone together with regime shifts towards humid conditions in the arid zone. Despite expanded TCZ sector, however, the available water resources inside it suffer little magnitude changes without preferential tendency towards either drier or wetter conditions, implying neither deleterious nor beneficial effects on the TCZ environment. Moreover, interannual variability of TCZ is expected to become stronger, resulting in more frequent occurrences of extreme swings. Finally, it is noted that uncertainty arising from climate models dominates in the TCZ than dispersed emission scenarios, in contrast to the situation in humid and arid zones.

✉ Gang Huang
hg@mail.iap.ac.cn

¹ Key Laboratory of Regional Climate-Environment for Temperate East Asia, Institute of Atmospheric Physics, Chinese Academy of Sciences, Beijing 100029, China

² Key Laboratory of Meteorological Disaster of Ministry of Education, Nanjing University of Information Science and Technology, Nanjing 210044, China

³ Center for Monsoon System Research, Institute of Atmospheric Physics, Chinese Academy of Sciences, Beijing 100190, China

⁴ State Key Laboratory of Numerical Modeling for Atmospheric Sciences and Geophysical Fluid Dynamics, Institute of Atmospheric Physics, Chinese Academy of Sciences, P.O. Box 9804, Beijing 100029, China

⁵ Joint Center for Global Change Studies, Beijing 100875, China

Keywords Transitional climate zone · East Asia · Vulnerability · Aridity index · Boundary (edge) · Dry-wet variation · Spatial swing

1 Introduction

Under the background of global warming, far-reaching, long-lasting and even devastating consequences are expected for planet Earth. Human-induced climate change increases extreme weather events, amplifies coastal erosion, melts glaciers and ice caps, puts pressure on ecosystems and in turn poses great threats to human society (Stocker et al. 2013). The global warming exerts pronounced influences via altering climate patterns worldwide. At present,

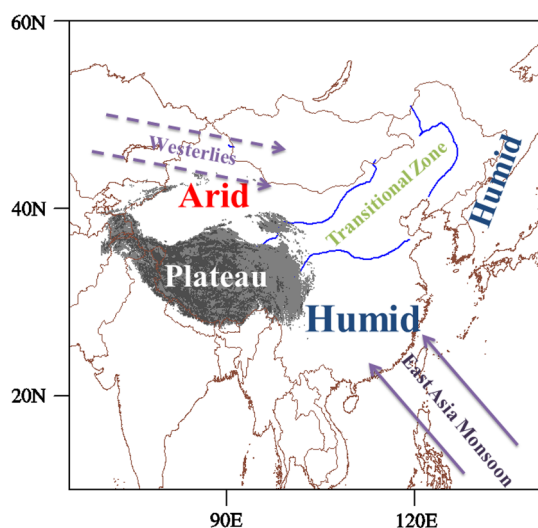
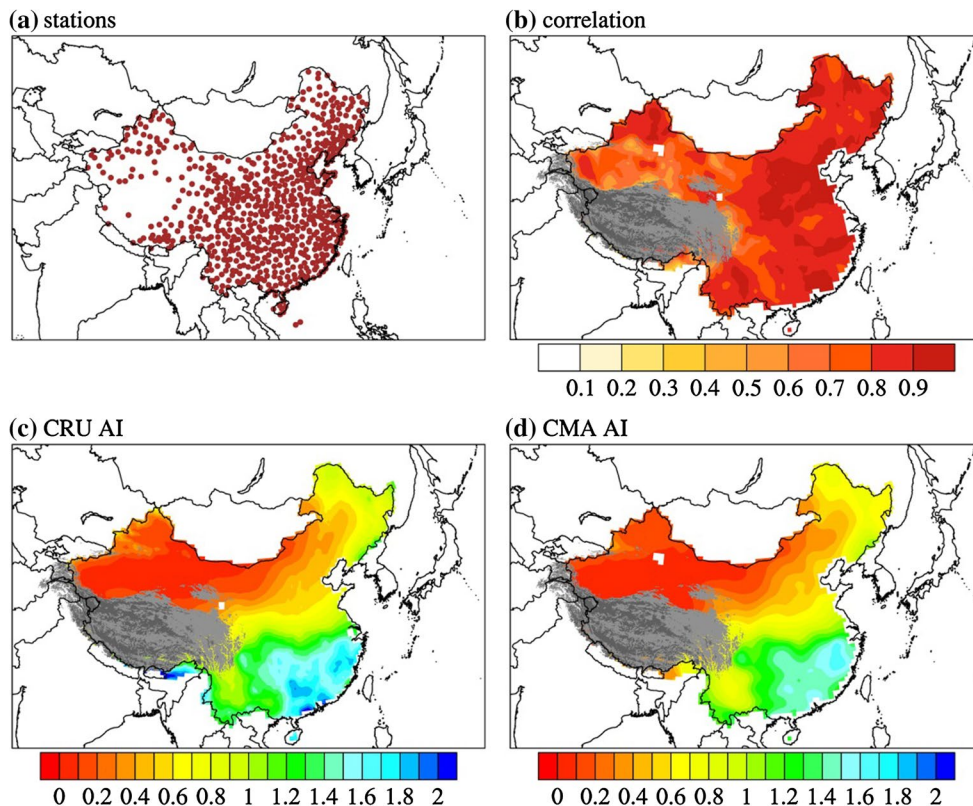


Fig. 1 The schematic illustration of the climatic zones and the dominant circulation systems controlling weather and climate in East Asia

assessments of climatic shifts over arid and monsoon humid zones in both historical and future perspectives have become hot topics. For example, Feng and Fu (2013) reports that global drylands have expanded in the last sixty

years and will continue to expand in the twenty-first century. Huang et al. (2016) shows by the end of twenty-first century drylands being will occupy half of the global land surface compared to 41 % coverage of present-day conditions. Similarly, Zhao et al. (2014) examine the simulation of historical and projected climate change in global arid and semiarid areas by CMIP5 models. From the regional perspective over East Asia, both Huo et al. (2013) and Liu et al. (2013) investigate the spatiotemporal changes of aridity index in the arid region of China and the underlying driving forces. Meanwhile, many studies have specifically targeted the issue of aridification in north China and its possible causes (Ma and Fu 2003; Ma 2007; Li et al. 2006). In parallel, numerous works have explored the dry-wet variability in global monsoon-affected domain across a wide range of temporal and spatial scales (Kitoh et al. 2013). For East Asian monsoon sector, Zhou et al. (2012) explored the implications of ENSO signal on South China Monsoon Climate. Wu and Wang (2002) and Chen et al. (2013) investigate the decadal changes in the relationship between ENSO and both the East Asian summer and winter monsoon. Huang et al. (2008) summarized progresses in studies of the temporal-spatial variations of the East Asian monsoon system and their impacts on climate anomalies in

Fig. 2 **a** Geographic locations of 756 meteorological stations in China; **b** spatial pattern of temporal correlation between AI of the CRU data and the CMA data; **c** AI climatology based on CRU data; **d** the same as **c**, but based on CMA data



China. Sun and Ding (2010) projects future change in summer precipitation and its associated monsoon circulation in East Asia, revealing a large increase of rainfall amount after 2040s. Indeed, there are plenty of studies concerning the variability and mechanism of East Asia Monsoon (i.e., Cui et al. 2008, 2009; Wang et al. 2014; Zhou et al. 2007a, b, c; Zuo et al. 2012, 2013).

However, significant attention is not given to the variation of the transitional climate zone (TCZ) in East Asia. In general, the transitional climate zone in East Asia is treated as southwest to northeast belt between desert arid and monsoon humid climates (Fig. 1). Despite relatively narrower spatial extent, this intercross zone is featured by large gradients of climate and biome (Fu 1992), interaction between

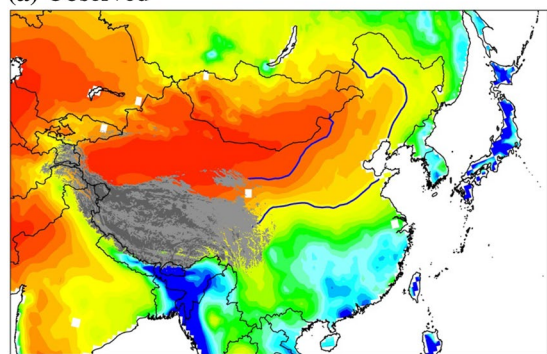
the East Asian summer monsoon and the mid-latitude westerly winds (Qian et al. 2009), and mixed cropping-pastoral activities (Shi 1996), all of which collectively makes it highly susceptible to natural disasters (Shi et al. 1994). In addition, the vegetation growth in this region is more unstable and sensitive to climate fluctuations (Ou and Qian 2006). In the past few years, parts of this knowledge gap have been bridged preliminarily: Ma et al. (2005) detect the historical variations of arid and semi-arid boundary in China at decadal time scale by using temperature-based Thornthwaite classification; Li and Ma (2013) investigate the dry-wet variability of climate zones based on 11 CMIP3 models under A1B scenario by using soil moisture. With these as ground work, this study is elaborated to advance

Table 1 Information of CMIP5 climate models employed in this study

Model acronym	Modeling center	Atmospheric component resolution (Lon. × Lat.)
ACCESS1-0	Commonwealth Scientific and Industrial Research Organization (CSIRO) and Bureau of Meteorology (BOM), Australia	1.875° × 1.25°
ACCESS1-3		1.875° × 1.25°
bcc-csm1-1	Beijing Climate Center, China Meteorological Administration, China	~2.8° × 2.8°
BNU-ESM	College of Global Change and Earth System Science, Beijing Normal University, China	~2.8° × 2.8°
CanESM2	Canadian Centre for Climate Modelling and Analysis, Canada	~2.8° × 2.8°
CESM1-BGC	Community Earth System Model Contributors, USA	1.25° × 0.9°
CNRM-CM5	Centre National de Recherches Météorologiques/Centre Européen de Recherche et Formation Avancées en Calcul Scientifique, France	~1.4° × 1.4°
CSIRO-Mk-3-6-0	Commonwealth Scientific and Industrial Research Organization in collaboration with the Queensland Climate Change Centre of Excellence, Australia	1.875° × 1.875°
GFDL-CM3	NOAA Geophysical Fluid Dynamics Laboratory, USA	2.5° × 2°
GFDL-ESM2G		2.5° × 2°
GFDL-ESM2 M		2.5° × 2°
GISS-E2-H	NASA Goddard Institute for Space Studies, USA	2.5° × 2°
GISS-E2-R		2.5° × 2°
HadGEM2-CC	Met Office Hadley Centre (additional HadGEM2-ES realizations contributed by Instituto Nacional de Pesquisas Espaciais), United Kingdom	1.875° × 1.25°
HadGEM2-ES		1.875° × 1.25°
inmcm4	Institute for Numerical Mathematics, Russia	2° × 1.5°
IPSL-CM5A-LR	Institut Pierre-Simon Laplace, France	3.75° × 1.875°
IPSL-CM5A-MR		2.5° × 1.25°
IPSL-CM5B-LR		3.75° × 1.875°
MIROC5	Atmosphere and Ocean Research Institute (The University of Tokyo), National Institute for Environmental Studies, and Japan Agency for Marine-Earth Science and Technology, Japan	~1.4° × 1.4°
MIROC-ESM	Japan Agency for Marine-Earth Science and Technology, Atmosphere and Ocean Research Institute (The University of Tokyo), and National Institute for Environmental Studies, Japan	~2.8° × 2.8°
MIROC-ESM-CHEM		~2.8° × 2.8°
MRI-CGCM3	Meteorological Research Institute, Japan	1.125° × 1.125°

our understanding of TCZ dynamics from both historical and future perspectives: first, this paper specifically concentrates on TCZ variability from multiple aspects, aiming to unravel not only the observed phenomenon but also underlying mechanism; second, future projection is assessed under the CMIP5 framework which is reported to generate relatively more realistic features than the preceding CMIP3 (Koutroulis et al. 2015); third, the climate types and boundaries are recognized by using widely known UNEP aridity index, which is considered to be better suited than soil moisture, since historical records of soil moisture are scarce as well as spatially sparse (Keyantash and Dracup, 2002) and what's more those retrieved from climate models has very large uncertainty (Li et al. 2007); last but not the least, the physically realistic Penman–Monteith model is adopted to infer potential evaporation (PET) rather than temperature-based Thornthwaite approach, which has been proven to overestimate PET especially under future warming climate (Burke et al. 2006).

(a) Observed



(b) Model

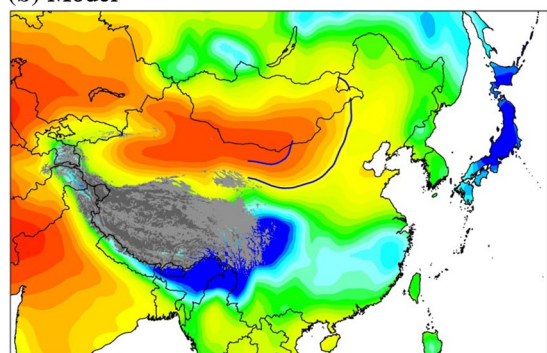


Fig. 3 Observed (a) and modeled (b) spatial distribution of the mean AI from 1961 to 2014 over East Asia, with blue colors being humid and red colors being arid. Transitional climate zone is enclosed by solid blue lines, while gray shaded area indicates Tibetan Plateau

This paper is organized as follows. Section 2 describes observational data sets and model simulations used in the study, together with the definition of transitional climate zone. Section 3 provides an overview of climatology and historical changes of the TCZ. Model's capability evaluation and future projections are elaborated in Sect. 4. Finally, Sect. 5 concludes the paper.

2 Data and methods

Monthly precipitation and potential evaporation (units: mm) amounts are retrieved from the Climatic Research Unit (CRU) version TS3.23 (Harris et al. 2014). Given relatively poor quality and low spatial density of in situ measurements in the earlier part of the twentieth century, we extracted the period from 1961 onwards of the full records. The grid extends over the global land of latitude 89.75°S to 89.75°N and longitude 179.75°W to 179.75°E, with a horizontal resolution of 0.5°. The CRU PET is derived based on Penman–Monteith scheme. Note that the CRU product is employed instead of station data accessible from meteorological observation network in China, because we focus on the domain of East Asia extending beyond China territory. Nevertheless, to verify the reliability of CRU gridded data, comparison is made with 756 gauge recordings (Fig. 2a) compiled by the China Meteorological Administration (CMA). For each site, precipitation is directly acquired while PET is estimated through the use of minimum and maximum temperature, wind speed, latitude, sunshine hours, elevation, actual vapor pressure, and surface pressure. As shown in Fig. 2c, d, it is found that the two datasets agree well in

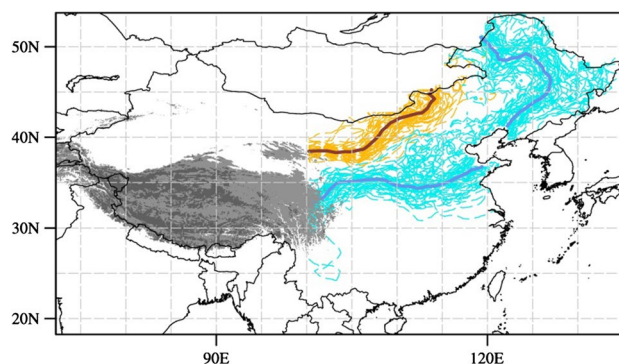


Fig. 4 Yearly front (thin blue) and rear (thin yellow) edges of TCZ during 1961 to 2014 and the average positions (bold blue and yellow)

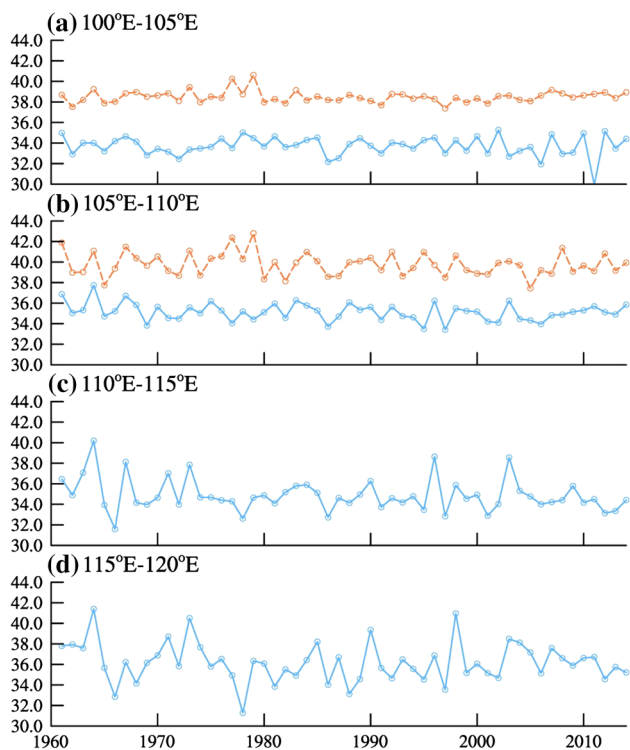


Fig. 5 Latitudinal variations of the front edge (*blue*) and rear edge (*yellow*) of TCZ along 100°E–105°E, 105°E–110°E, 110°E–115°E, 115°E–120°E

the large-scale configuration of AI climatology in East Asia with pattern correlation above 0.95. Moreover, these two datasets generate temporal coherent AI fields, since most of the grid cells have very high correlation coefficients greater than 0.8 (Fig. 2b). Consequently, the result strongly supports the use of CRU data.

Simulated climates of historical period and future projections under two emissions scenarios, Representative Concentration Pathway (RCP) 4.5 (medium mitigation scenario) and RCP8.5 (high emission scenario) (Moss et al. 2010) are obtained from the World Climate Research Programme (WCRP) Coupled Model Intercomparison Project Phase 5 (CMIP5) (Taylor et al. 2012). Our study uses 23 coupled model outputs spanning from 1961 to 2099, as listed in Table 1. Retrieved variables encompass near-surface air temperature including mean, minimum, and maximum, surface pressure, wind speed at 10 m, surface downwelling shortwave radiation, surface upwelling shortwave radiation, surface downwelling longwave radiation, surface upwelling longwave radiation, and near-surface relative humidity together with precipitation. All above quantities except precipitation are used as input parameters to calculate the PET. Because of spatial resolutions varying from model to model, bilinear interpolation is adopted to regrid all the modeled climate fields to match that of CRU data source.

Fig. 6 Longitudinal variations of the front edge (*blue*) and rear edge (*yellow*) of TCZ along 40°N–45°N, 45°N–50°N

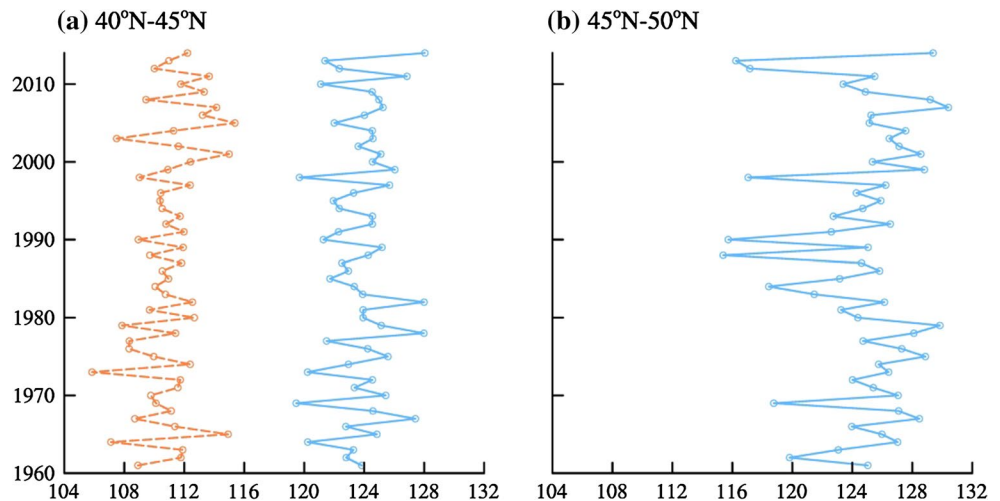
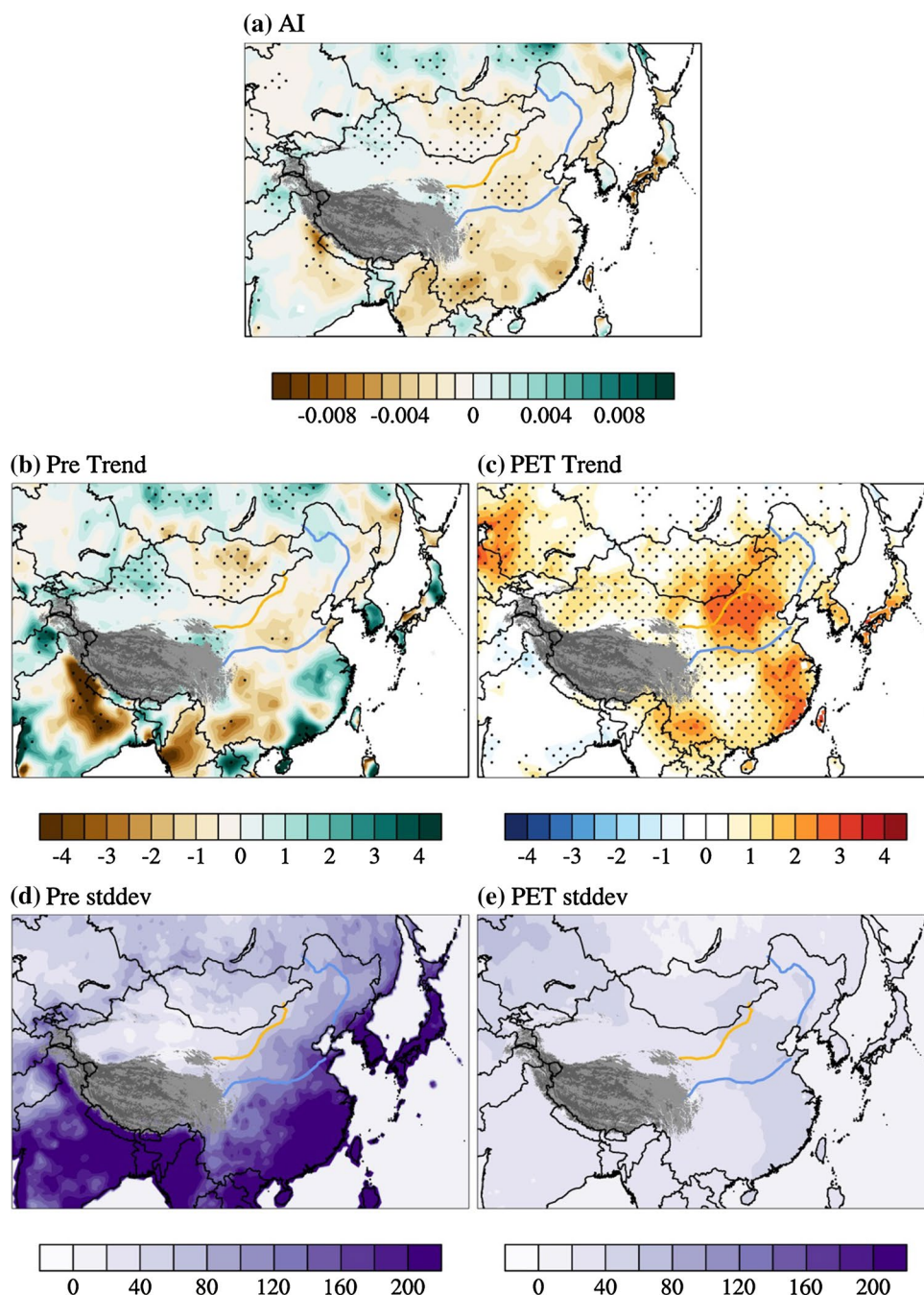


Fig. 7 Spatial pattern of AI trend (a, unit: yr^{-1}), precipitation trend (b, unit: mm/yr), PET trend (c, unit: mm/yr), standard deviation of precipitation (d) and PET (e, unit: mm) with linear trend removed. Grid boxes where the trend is significant at the 10 % level are indicated by black dots



Aridity Index (AI) serves as basis for the delineation of climate types. The AI is defined as the ratio of annual precipitation sum to annual PET sum, which essentially indicates the precipitation availability over atmospheric water demand (UNEP 1997). Here, the PET is parameterized through Penman–Monteith equation as detailed

in Allen et al. (1994), which is considered to be more physically realistic and recommended by the Food and Agriculture Organization (FAO) of the United Nations. According to the values of AI, the climate is categorized as Arid ($\text{AI} < 0.2$), Semi-Arid ($0.2 < \text{AI} < 0.5$), Dry sub-humid ($0.5 < \text{AI} < 0.65$) and Humid ($\text{AI} > 0.65$). The

term “transitional zone” ($0.2 < AI < 0.65$) refers to a combination of Semi-Arid and Dry subhumid environments, as an intermediate between arid and humid climates. Furthermore, the 0.65 and 0.2 AI isolines correspond to the front and rear limits of transitional zone, respectively.

3 Climatology and historical variation of the TCZ in East Asia

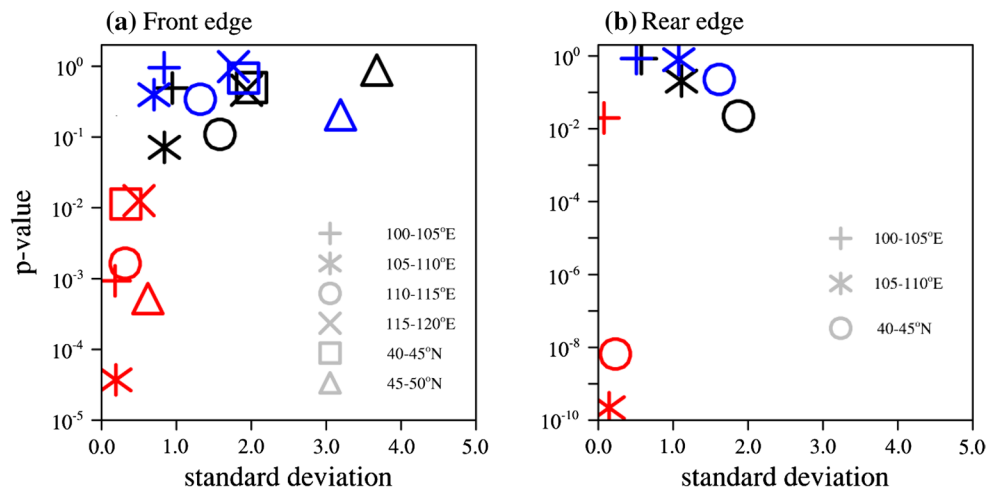
Figure 3a depicts spatial distribution of AI climatology, with the heavier isolines 0.2 and 0.65 highlighting the boundaries of TCZ. The AI generally decreases from the south and the east toward the interiors, with the southeastern part of China, Korean Peninsula, Japan and part of Northeast Asia under humid conditions whereas Northwest China and the southern part of Mongolia being arid lands. The transition belt, outlined by bold blue lines, geographically stretches across the northern China in a northeast-southwest orientation from the eastern fringe of Tibetan Plateau to the western Northeast China, covering an area of about $1.8 \times 10^6 \text{ km}^2$. The most prominent features are that this zone harbors sharp gradient from humid to arid regimes and the width broadens from west to east. Note that although other areas may meet the criterion $0.2 < AI < 0.65$, those are not pertinent to the marginal influence of East Asia summer monsoon; that is, the realm we consider is not only humid-to-arid transition zone but also monsoon-to-non-monsoon transition zone.

Figure 4 illustrates the yearly elongations of front and rear edges of the TCZ, along with their respective climatological positions. There appears to be wide year-to-year excursions of both edges, with the greatest deviation from the norm by as much as 9° . In addition, the eastern part of TCZ is characterized by larger spatial swings (also see Fig. 8). In short, the domain of TCZ in East Asia is subjected to strong interannual variability. To facilitate further analysis, the edge of TCZ is partitioned into multiple segments of 5° span and then the temporal behavior of each segment is presented respectively, as shown in Figs. 5 and 6. Whether the latitudinal or longitudinal oscillation is being investigated depends on their relative importance: for example, the front edge in $100\text{--}105^\circ\text{E}$ varies primarily in meridional direction, so that extracting latitudinal information appears to be feasible and meaningful.

On the one hand, the eastmost section exhibits strongest interannual variability whose standard deviation reaches to 3.67° and 1.97° for the front and rear edges respectively, while conversely those toward the west are more stable with a relatively small standard deviation (Fig. 8). On the other hand, the rear edge has more moderate amplitude of spatial swings comparing with the front one, suggesting damped climate sensitivity as latitudes increase; nevertheless, despite differences in magnitude, they share some degree of temporal coherence, with correlation coefficients being around 0.3.

In a long-term context, both the front and rear edges have experienced coastward migration, although only the trends in $105\text{--}110^\circ\text{E}$, $110\text{--}115^\circ\text{E}$ bands of front edge and $40\text{--}45^\circ\text{N}$ band of rear edge are statistically significant

Fig. 8 *p* value of linear trend and standard deviation (with the linear trend removed, unit: $^\circ$) in each segment of TCZ boundaries (the left plot for front edge, while the right one rear edge). Each segment is stamped by different marker symbol (legend information). Individual and combined impacts of precipitation and PET on the relevant statistics are colored in blue, red and black (also real world), respectively. Note that the smaller the *p* value, the more significant the trend is, and that Y-axis ranges are different between two drawings



at 10 % level. The maximum shift rate reaches to 0.02° southward per year occurring around $110\text{--}115^\circ\text{E}$ for the front edge and 0.04° eastward per year occurring around $40\text{--}45^\circ\text{N}$ for the rear edge, respectively. To gain better understanding of the forces driving TCZ-boundary tendency, Fig. 7 is created to show the spatial pattern of AI, precipitation and PET trends. As seen in Fig. 7a, the

coastward migration of TCZ is exactly caused by the notable decreasing AI over the extended area from Mongolia to central China. Besides, subplots (b) and (c) suggest that a decrease in precipitation and an increase of PET jointly translate into decreasing AI values. Furthermore, not only are the TCZ edges expected to southeastward shift, but the moist state inside it also appears to have become more arid,

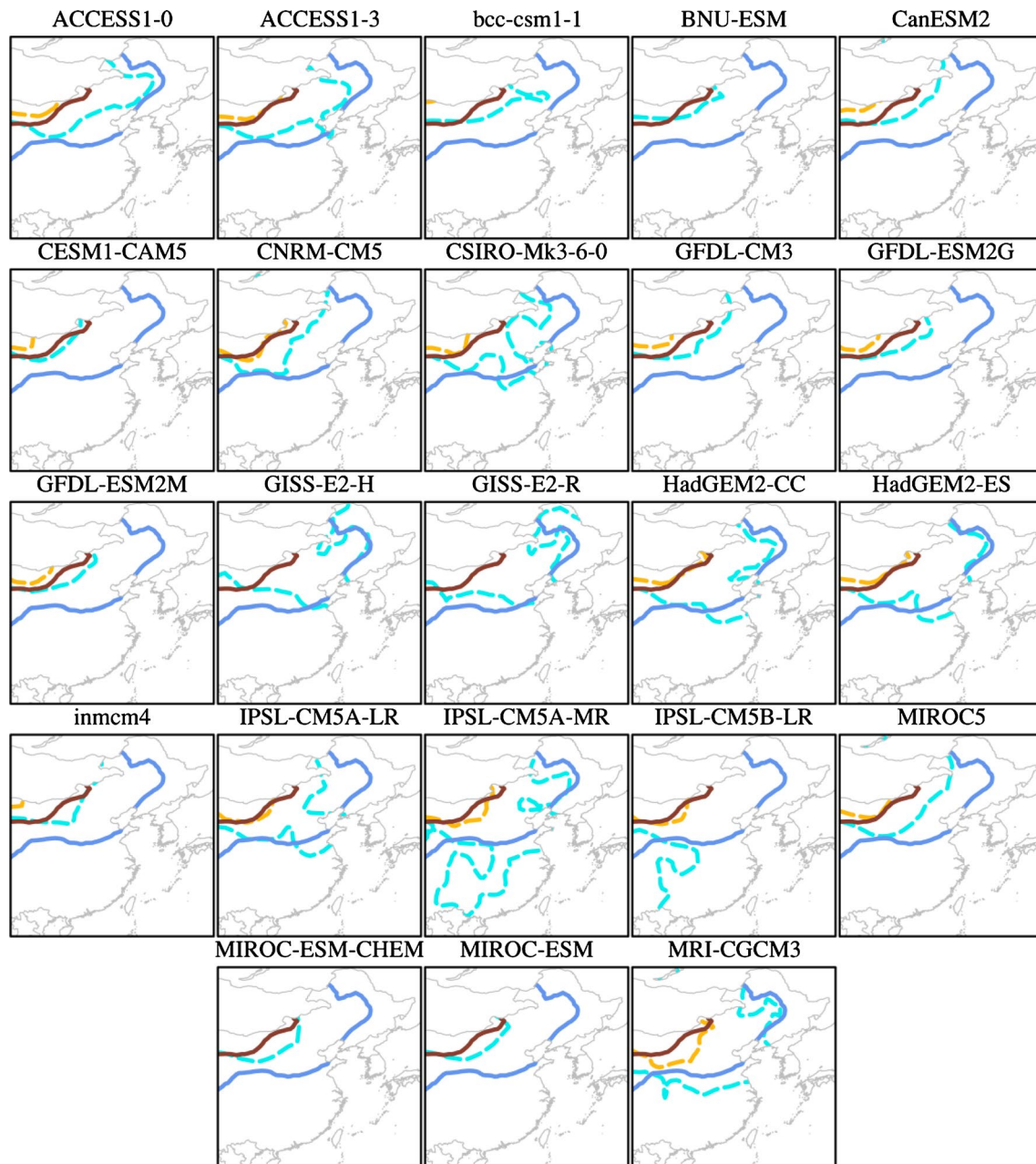


Fig. 9 Climatological front (dashed blue) and rear edges (dashed brown) of TCZ for individual climate model simulations compared against observations (solid lines)

as the TCZ-domain averaged AI decrease at a rate of 0.001 per year at 10 % significant level with the strongest deterioration in the central part.

To isolate the role of precipitation and PET in shaping the morphology of TCZ, the spatial extent of TCZ is re-built by prescribing the climatological precipitation or PET, as illustrated in Fig. 8. When effect from precipitation is removed, merely detected is the long-term trend of southeast displacement without apparent interannual signal; moreover, the trends of edge location for all segments are significant at 90 % confidence level. In contrast, the time series driven by precipitation fluctuate drastically over the period, but the long-term tendency is virtually indistinctive. In addition, Fig. 7b–e directly compare the properties of precipitation versus PET in terms of trend and standard deviation. Contrasting Fig. 7b, c, an evident signal of enhanced PET emerges around the TCZ, but there is small and insignificant reduction in precipitation; however, when we turn to the standard deviation (Fig. 7d, e), the amplitude of precipitation oscillation is 2–3 times larger than that of PET. In short, thus, the precipitation makes a large contribution to interannual variance, while the long-term trend is regulated mainly by the PET, and thereby the coupling of precipitation and PET reproduces the realistic type of variability.

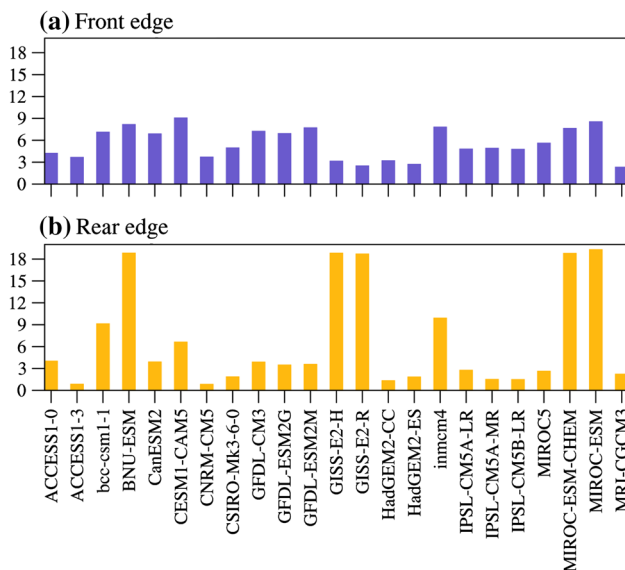


Fig. 10 The root mean square error (unit: °) in simulating front (a) and rear edge (b) for each CMIP5 model. Note that lower RMSE scores values correspond to better skill in representing TCZ boundaries

4 Future projected changes of TCZ

Prior to carrying out future projections, we first evaluate CMIP5 models' performance in simulating the domain of TCZ, the practice of which is essential to confidence rating in model-based projection and bias adjustment. Figure 3b shows spatial pattern of multimodel averaged AI with blue lines to demarcate climatic zone limits. Further, Figs. 9 and 10 provide an in-depth view of individual model capability and its associated root mean square error (RMSE) metric score. Generally, the majority of models features a northwestward shifted TCZ with smaller area relative to the observed one, especially for its front boundary. In other words, model overestimates the extent of humid zone and to a lesser degree displaces the dry environment towards deeper inland. Despite the position bias, the current generation of models with a few exceptions (IPSL-CM5A-MR and IPSL-CM5B-LR) is able to effectively reproduce the shape and orientation of TCZ. Based on RMSE scores reported in Fig. 10, on the one hand, ACCESS1-3, GISS-E2-R, HadGEM2-CC, HadGEM2-ES and MRI-CGCM3 show superior skill at representing the front boundary of TCZ; on the other hand, ACCESS1-3, CNRM-CM5, HadGEM2-CC, IPSL-CM5A-MR and IPSL-CM5B-LR are identified as well-performing models with regard to the rear edge. Combine the two ranks by summation, we note that ACCESS1-3, HadGEM2-CC, HadGEM2-ES and MRI-CGCM3 exhibit highest skill in replicating the TCZ passage as well as dry condition to the northwest and moist condition to the southeast. In addition, the CMIP5 models are found to simulate rear edge location better than the front one.

Although the climate models have an acceptable level of performance, it is still necessary to implement bias correction procedure to reduce the systematic errors. In recent years, numerous bias correction methods of varying algorithm and complexity have been developed, as summarized in Teutschbein and Seibert (2012). Although sophisticated techniques are available, the simple scaling strategy is preferred in this study because of its simplicity and straightforward manner. Scaling adjustment acts to scale model data by the quotient between the mean of the observations and the simulation in the reference period:

$$AI_{bc-mod}(t) = AI_{raw-mod}(t) \times (\overline{AI}_{obs} / \overline{AI}_{raw-mod})$$

where $AI_{raw-mod}(t)$ and $AI_{bc-mod}(t)$ are the raw and bias-corrected AI for model at time node t , and \overline{AI}_{obs} and $\overline{AI}_{raw-mod}$ denotes the climatological mean of observed and modeled AI in the calibration period (1961–1990 here).

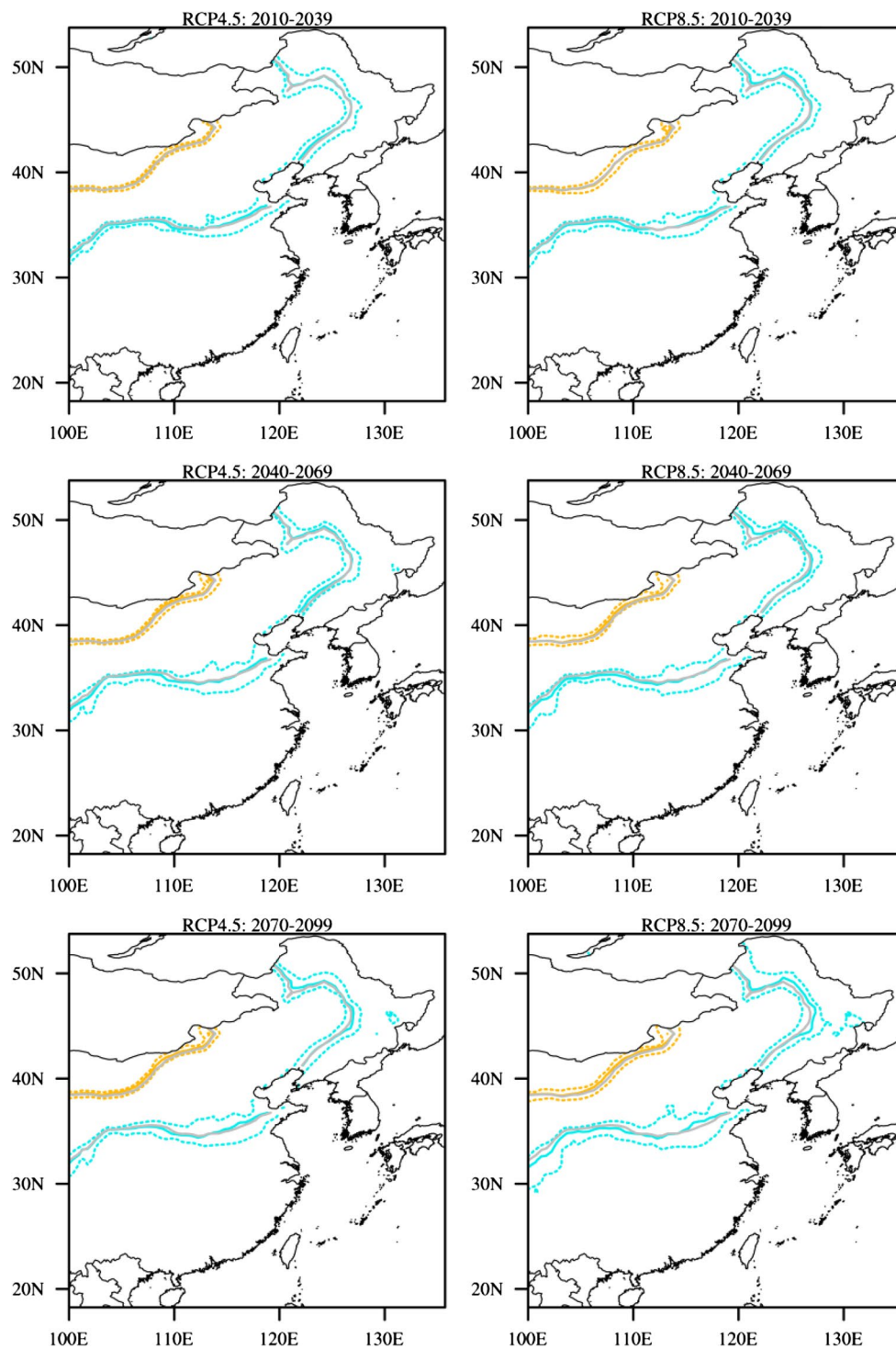


Fig. 11 Projected movements of front (blue) and rear (yellow) edges of TCZ over East Asia for 2010–2039 (top row), 2040–2069 (middle row) and 2070–2099 (bottom row) under RCP4.5 (left column) and

RCP8.5 (right column). The solid blue and yellow lines indicate the ensemble-mean, while the dashed ones mark 20–80 % likelihood range. The 1961–1990 baseline is superimposed as a gray line

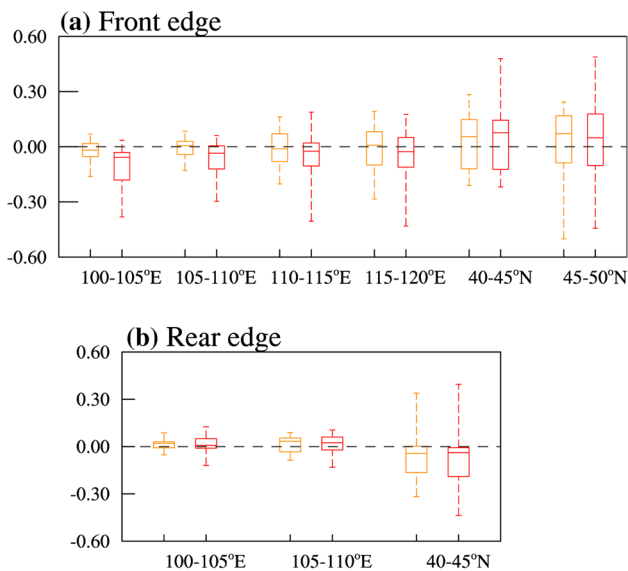


Fig. 12 Box plots of the trends in front (a) and rear (b) edge of all models between 1990 and 2099 (unit: $^{\circ}$ /decade) under RCP4.5 (yellow) and RCP8.5 (red). In the box plot, the line in the middle of the box, lower and upper bound of the box represent median, 25 and 75 percentiles, respectively; the top and bottom whiskers extend to the maximum and minimum values

After applying bias correction, the bias-corrected modeled data share identical mean climate with observations in the reference period, and at the same time the climate change signal is preserved.

Figures 11, 12, 13, 14 and 15 collectively illuminate projected future dynamics of the climatic zones' boundary and dryness-wetness change information specific to each zone, with emphasis on the TCZ. At first, Fig. 11 depicts spatially shifting pattern of the TCZ for three 30-year intervals under RCP4.5 and RCP8.5; however, because the small-scale details are almost illegible in the context of large domain, complementary Fig. 12 is provided, in which the linear trend and uncertainty range are individually derived for every 5° -segments. In terms of multimodel ensemble mean, the front edge of TCZ is linked to a southeastward migration, while the opposite northwestward movement is predicted for the rear one, resulting in expansion of TCZ area accompanied by shrinking of humid zone and retreat of arid zone. Models also reveal that the most substantial shift of about 0.75° takes place over the westmost side of the front edge during 2070–2099 under RCP8.5, and the shift of front edge is two times faster than the rear one. However, these projections show a visible spread among the models, with the interquartile span of the ensembles ranging from

0.2° to 3° . In comparative terms, the uncertainty envelopes associated with the front edge is about double wider than that with the rear one. Although models do not achieve uniform consensus on the future behavior of the entire TCZ, consistent projections do exist in several portions. It is found that the movements tied to $100\text{--}105^{\circ}\text{E}$ and $105\text{--}110^{\circ}\text{E}$ under RCP8.5 along the front edge, and $100\text{--}105^{\circ}\text{E}$ under RCP4.5 and $40\text{--}45^{\circ}\text{N}$ under both RCP scenarios along the rear edge correspond to an agreement on sign amongst at least 75 % of models. Moreover, it is noteworthy that high emission scenario not only magnifies the amplitude of these tendencies, but also produces higher level of inter-model spread. Nevertheless, the scenario uncertainty is much smaller than the model uncertainty.

Since comprehensive assessment of projections desires the need to go beyond mean and trend statistics, Fig. 13 is made to infer probability distribution changes from projections of multiple models. It can be seen that the changes in probability curve is not related to the shift of mean state or the shape. Rather, either the right- or left-side tail (or both) will become fatter with concurrently smaller peak frequency, reflecting that the boundary lines will be more often farer away from the mean. The most significant changes in probability are seen in the $100\text{--}105^{\circ}\text{E}$ and $105\text{--}110^{\circ}\text{E}$ of the front edge and $105\text{--}110^{\circ}\text{E}$ and $40\text{--}45^{\circ}\text{N}$ of the rear edge, in line with the trend outcomes reported in Fig. 12, while others are characterized by a slight tendency to a broader distribution. In short, the increased chances of extreme TCZ swings are expected in future.

Figures 14 and 15 are designed to uncover the driving forces underlying the future scenarios of TCZ. Figure 14 presents the spatial pattern of projected changes in the AI, expressed as percentage (%) from the reference period. East Asia exhibits a strong contrast in projected AI changes, with large increase in the northwest and large decrease in both the southeast and northeast, which alleviates the water deficit in desert zone and exerts moisture stress in humid region. Moreover, there is generally good agreement between different models in terms of the direction of AI changes. Such anticipated changes can be summarized into a simple rule “wet get drier, dry get wetter”, as opposed to the classic paradigm “wet get wetter, dry get drier” (Held and Soden, 2006). Therefore, the spacious drying and wetting tendencies in humid and arid zones are responsible for the southeastward and northwestward shift of the front and rear edge of TCZ, respectively. Conversely, it seems to be no appreciable changes in the TCZ, although confidence

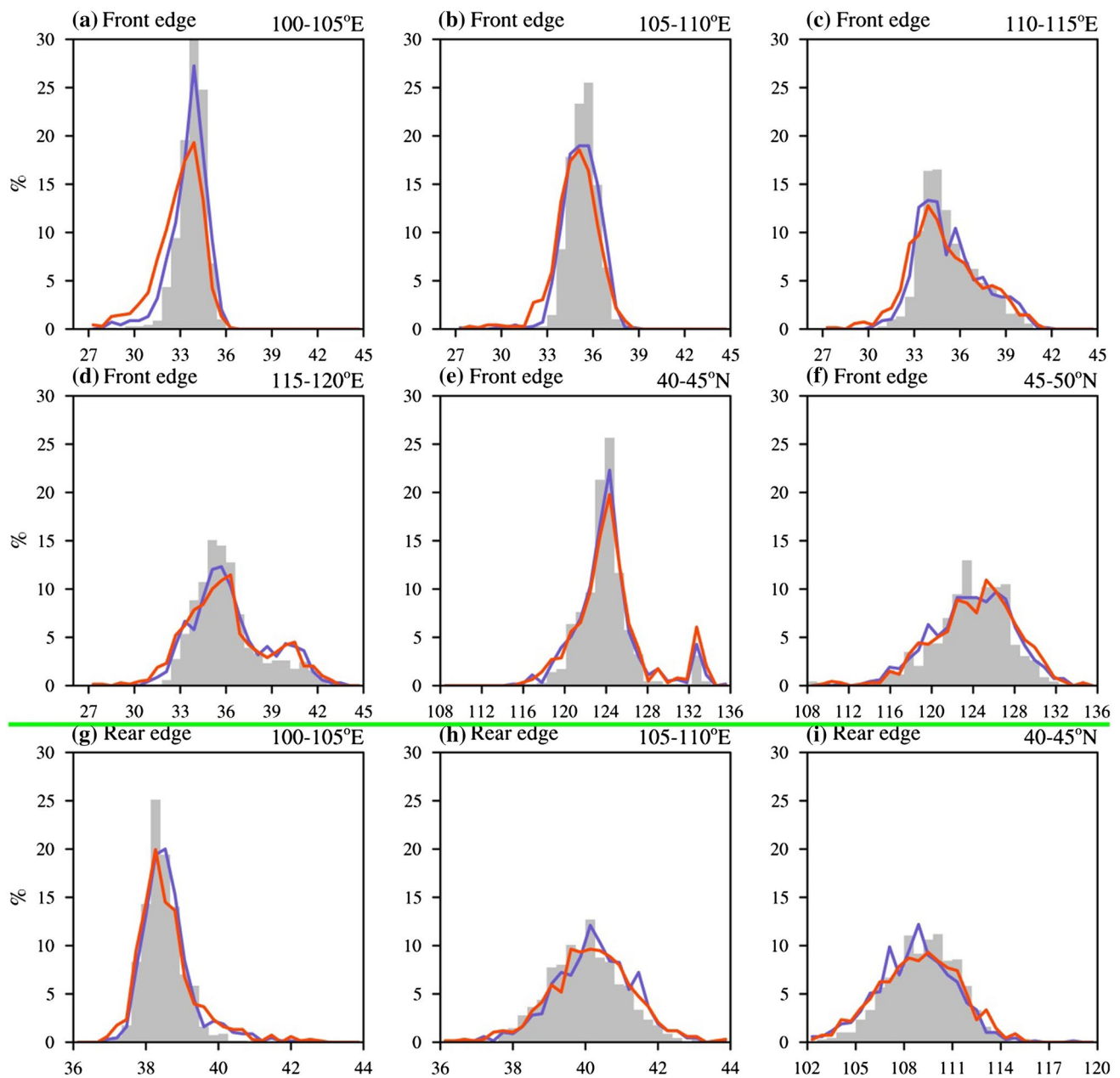


Fig. 13 Probability distribution of TCZ boundaries for baseline (1961–1990, gray bar) and the end-of-twenty-first century (2070–2099, solid lines) under RCP4.5 (blue) and RCP8.5 (red). Results are presented for every 5°-segments of the front (a–f) and rear (g–i) boundaries

about drying or wetting is relatively low. Figure 15 portrays the regionally averaged AI in the future for the humid, transitional and arid zones, respectively. On the one hand, albeit differ in the magnitude, climate models are unanimous in projecting future drying tendency in the humid zone, with 7 % AI drop for RCP4.5 and 13 % AI drop for RCP8.5 by the end of the twenty-first century with respect to historical condition. Therefore, the

water rich region is likely to be water-stressed and more prone to drought in the future, but even so, it is still possess enough humidity to stay in “humid category”. On the other hand, drylands will steadily receive more available water, which is of vital importance to mitigate the burden of water scarcity. Note that in spite of very small absolute changes, the percentage change can be greater than 10 %. Instead of pronounced changes as noted in

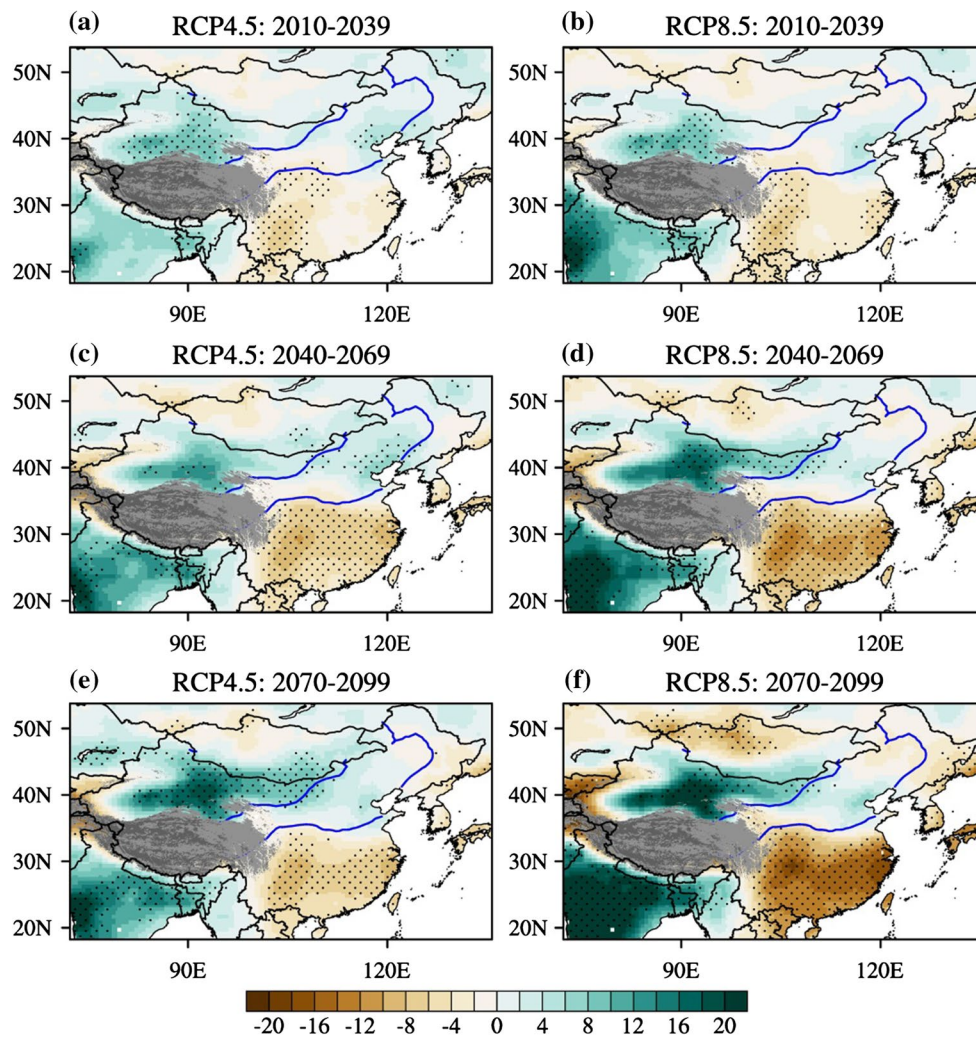


Fig. 14 CMIP5 multi-model ensemble average percent change (unit: %) in Aridity Index for 2010–2039 (1st row), 2040–2069 (2nd row) and 2070–2099 (3rd row) compared to 1961–1990 baseline cli-

mate under RCP4.5 (1st column) and RCP8.5 (2nd column). Stippling illustrates agreement in sign of changes across at least 70 % models, and the thick blue line encloses the TCZ domain in baseline climate

the humid and arid zones, however, there is no clear preference for either becoming drier or wetter in the TCZ, since AI remains quite stable at 0.45 with narrow model dispersion throughout the twenty-first century. In brief summary, the joint effect of remarkable water loss in the humid zone and gain in the arid zone favors the southeastward departure of TCZ front edge as well as the opposite response of TCZ rear edge, but the water resources inside the TCZ remains invariant with time and emission scenarios.

Finally, extra effort is devoted to consolidate the above findings obtained. It is bias-corrected models data that are

used to build future projections, due to the common deficiency in the simulated position of TCZ. However, the composite of top-performing models ranked by the RMSE scores (Fig. 10) does a good job at representing TCZ in terms of not only shape-orientation but also position (figure not shown), which encourages us to re-examine the projections with the raw outputs of high skill models. The result suggest that best models' ensemble without bias adjustment and all models' ensemble processed by bias correction yield essentially identical outcomes (figures not shown), which gives us more confidence in the conclusions.

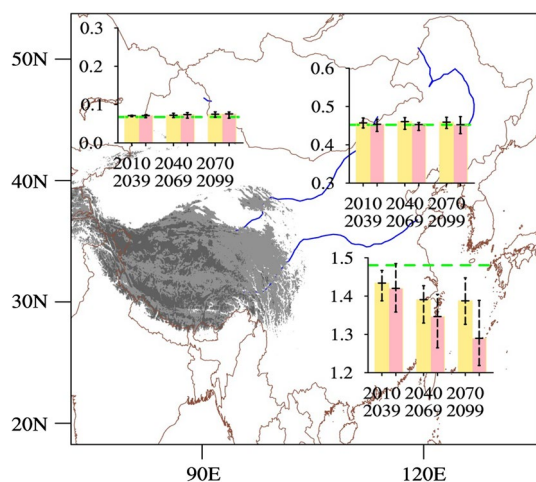


Fig. 15 Projected aridity index averaged over arid, transitional and humid zones (from *top-left* to *bottom-right*) during 2010–2039, 2040–2069 and 2070–2099 under RCP4.5 (yellow bar) and RCP8.5 (pink bar). The error bar denotes the 25–75 % confidence interval, and the green dashed line represents the 1961–1990 climatology

5 Conclusions

The TCZ in East Asia, situated between humid climate conditions to the southeast and northeast and desert dry conditions to the northwest, stretches from the east fringe of the Tibetan Plateau to the west of Northeast China. This belt is considered to be “interface fragile” to natural disasters and climatic changes, owing to the steep gradients of climate and biome systems, interaction between the East Asian summer monsoon and westerly winds, and mixed agriculture-pasture activities. However, most of earlier studies focused on the effects of climate change on monsoon humid region and drylands, so that more efforts are needed to illuminate the spatial and temporal behaviors of TCZ in response to global warming. Therefore, this study conducts a more focused and detailed survey of TCZ.

From a historical perspective, both front and rear edges exhibit dramatic spatial swings, with greater excursion occurring at a more east longitude. In addition, the front edge exhibit higher amplitude of deviation than the rear one. During the past 54 years, the TCZ sector has undergone coastward displacement, which can be interpreted as a consequence of progressively drop in AI in response to collaborative forcing of reduced precipitation and enhanced PET over the extended area from Mongolia to central China. Furthermore, not only are the TCZ edges expected to southeastward shift, but the moisture condition inside it has evolved towards greater aridity. By disentangling the effects of precipitation and PET, we find that a rapid increase of PET excites the southeastward shift of TCZ

while precipitation fluctuation is the dominant driver of interannual variability.

Although the TCZ in CMIP5 shift northwest to its real position, most models are able to reproduce the broad pattern of TCZ. In particular, ACCESS1-3, HadGEM2-CC, HadGEM2-ES and MRI-CGCM3 stand out as well-performing models. To minimize the bias, models’ output is statistically adjusted via simple scaling technique.

In the twenty-first century, the front edge of TCZ is expected to continue to shift southeastward, while the rear edge responds in an opposite manner. This result implies an expansion of TCZ sector, along with contraction of the humid zone and northwestward retreat of the drylands. It is confirmed that the wet regions getting drier and the dry regions getting wetter causes the future tendency of TCZ boundaries. However, although significant responses are seen within humid and arid zones, the available moisture inside the TCZ does not change that much, without preferential inclination towards either drier or wetter conditions. Hence, projections assume no deteriorated and beneficial effects of climate change on the TCZ environment. Moreover, the TCZ boundaries in future are more prone to stronger swings, suggesting more drastic dry-wet variability in surrounding regions.

Acknowledgments We thank the reviewers for their constructive comments on the manuscript. This work was supported by the National Natural Science Foundation of China Grant No. 41461144001, the National Key Research and Development Program of China Grant No. 2016YFA0600604, the National Outstanding Youth Science Fund Projection of China Grant No. 41425019, the National Natural Science Foundation of China Grants Nos. 91337105, 41505069, 41275083 and 41530425, Public science and technology research funds projects of ocean Grant No. 201505013, and Open Research Fund Program of Key Laboratory of Meteorological Disaster of Ministry of Education (Nanjing University of Information Science and Technology) Grant No. KLME1403.

References

- Allen RG, Smith M, Pereira A, Perrier LS (1994) An update for the calculation of reference evapotranspiration. *ICID Bull* 43(2):1–34
- Burke EJ, Brown SJ, Christidis N (2006) Modeling the recent evolution of global drought and projections for the twenty-first century with the Hadley Centre climate model. *J Hydrometeorol* 7(5):1113–1125
- Chen W, Feng J, Wu R (2013) Roles of ENSO and PDO in the linkage of the East Asian winter monsoon to the following summer monsoon. *J Clim* 26(2):622–635
- Cui X, Huang G, Chen W (2008) Notes of regional climate model simulation for hydrological studies in China. *Adv Atmos Sci* 25:999–1008
- Cui X, Huang G, Chen W, Morse A (2009) Threatening of climate change on water resources and supply: case study of North China. *Desalination* 248:476–478

- Feng S, Fu Q (2013) Expansion of global drylands under a warming climate. *Atmos Chem Phys* 13(10):10081–10094
- Fu C (1992) Transitional climate zones and biome boundaries: a case study from China. In: Hansen AJ, Castri FD (eds) *Landscape Boundaries*. Springer-Verlag, New York, pp 394–402
- Harris I, Jones PD, Osborn TJ, Lister DH (2014) Updated high-resolution grids of monthly climatic observations—the CRU TS3. 10 Dataset. *Int J Climatol* 34(3):623–642
- Held IM, Soden BJ (2006) Robust responses of the hydrological cycle to global warming. *J Clim* 19(21):5686–5699
- Huang R, Gu L, Chen J, Huang G (2008) Recent progresses in studies of the temporal-spatial variations of the East Asian monsoon system and their impacts on climate anomalies in China. *Chin J Atmos Sci* 32(4):691–719 (in Chinese)
- Huang J, Yu H, Guan X, Wang G, Guo R (2016) Accelerated dryland expansion under climate change. *Nat Clim Change* 6:166–171
- Huo Z, Dai X, Feng S, Kang S, Huang G (2013) Effect of climate change on reference evapotranspiration and aridity index in arid region of China. *J Hydrol* 492:24–34
- Keyantash J, Dracup JA (2002) The quantification of drought: an evaluation of drought indices. *Bull Am Meteorol Soc* 83(8):1167–1180
- Kitoh A, Endo H, Krishna Kumar K, Cavalcanti IF, Goswami P, Zhou T (2013) Monsoons in a changing world: a regional perspective in a global context. *J Geophys Res Atmos* 118(8):3053–3065
- Koutroulis AG, Grillakis MG, Tsanis IK, Papadimitriou L (2015) Evaluation of precipitation and temperature simulation performance of the CMIP3 and CMIP5 historical experiments. *Clim Dyn*. doi:10.1007/s00382-015-2938-x
- Li M, Ma Z (2013) Soil moisture-based study of the variability of dry-wet climate and climate zones in China. *Chin Sci Bull* 58:531–544
- Li X, Ma Z, Liu X (2006) Inter-decadal characteristics of aridification over northern China in association with variations of the atmospheric circulation during the last fifty years. *Chin J Atmos Sci* 30(2):277–284 (in Chinese)
- Li H, Robock A, Wild M (2007) Evaluation of Intergovernmental Panel on Climate Change Fourth Assessment soil moisture simulations for the second half of the twentieth century. *J Geophys Res Atmos* 112(D6):2007
- Liu X, Zhang D, Luo Y, Liu C (2013) Spatial and temporal changes in aridity index in northwest China: 1960 to 2010. *Theor Appl Climatol* 112(1–2):307–316
- Ma Z (2007) The interdecadal trend and shift of dry/wet over the central part of North China and their relationship to the Pacific Decadal Oscillation (PDO). *Chin Sci Bull* 52(15):2130–2139
- Ma Z, Fu C (2003) Interannual characteristics of the surface hydrological variables over the arid and semi-arid areas of northern China. *Global Planet Change* 37(3):189–200
- Ma Z, Fu C, Dan L (2005) Decadal variations of arid and semi-arid boundary in China. *Chin J Geophys* 48:574–581
- Middleton N, Thomas D (1997) *World atlas of desertification*, 2nd edn. Edward Arnold for United Nations Environment Programme, Nairobi/London
- Moss RH, Edmonds JA, Hibbard KA, Manning MR, Rose SK, Van Vuuren DP, Carter TR, Emori S, Kainuma M, Kram T, Meehl GA (2010) The next generation of scenarios for climate change research and assessment. *Nature* 463(7282):747–756
- Ou T, Qian W (2006) Vegetation variations along the monsoon boundary zone in East Asia. *Chin J Geophys* 49(3):627–636
- Qian W, Ding T, Hu H, Lin X, Qin A (2009) An overview of dry-wet climate variability among monsoon-westerly regions and the monsoon northernmost marginal active zone in China. *Adv Atmos Sci* 26:630–641
- Shi Z (1996) Regional characters of natural disaster in marginal monsoon belt of China. *J Arid Land Resour Environ* 10(4):1–7 (in Chinese)
- Shi Z, Zhang L, Sui G (1994) Natural disasters and their formation causes on Chinese monsoon marginal belt. *J Catastrophol* 9(4):59–64 (in Chinese)
- Stocker TF, Qin D, Plattner GK, Tignor M, Allen SK, Boschung J, Nauels A, Xia Y, Bex B, Midgley BM (2013) *The Physical Science Basis. Contribution of Working Group I to the Fifth Assessment Report of the Intergovernmental Panel on Climate Change*. Cambridge University Press, Cambridge
- Sun Y, Ding Y (2010) A projection of future changes in summer precipitation and monsoon in East Asia. *Sci China Earth Sci* 53(2):284–300
- Taylor KE, Stouffer RJ, Meehl GA (2012) An overview of CMIP5 and the experiment design. *Bull Am Meteor Soc* 93:485–498
- Teutschbein C, Seibert J (2012) Bias correction of regional climate model simulations for hydrological climate-change impact studies: review and evaluation of different methods. *J Hydrol* 456:12–29
- Wang F, Yang S, Higgins W, Li Q, Zuo Z (2014) Long-term changes in total and extreme precipitation over China and the US and their links to oceanic-atmospheric features. *Int J Climatol* 34:286–302
- Wu R, Wang B (2002) A contrast of the East Asian summer monsoon and ENSO relationship between 1962–77 and 1978–93. *J Clim* 15:3266–3279
- Zhao T, Chen L, Ma Z (2014) Simulation of historical and projected climate change in arid and semiarid areas by CMIP5 models. *Chin Sci Bull* 59(4):412–429
- Zhou W, Chan JCL (2007) ENSO and South China Sea summer monsoon onset. *Int J Climatol* 27:157–167
- Zhou W, Li CY, Wang X (2007a) Possible connection between Pacific oceanic interdecadal pathway and East Asian winter monsoon. *Geophys Res Lett* 34:L01701
- Zhou W, Wang X, Zhou T, Li CY, Chan JCL (2007b) Interdecadal variability of the relationship between the East Asian winter monsoon and ENSO. *Meteorol Atmos Phys* 98:283–293
- Zhou W, Chen W, Wang D (2012) The implications of ENSO signal for South China monsoon climate. *Aquat Ecosyst Health Manag Soc* 15(1):14–19
- Zuo Z, Yang S, Kumar A, Zhang R, Xue Y, Jha B (2012) Role of thermal condition over Asia in the weakening Asian summer monsoon under global warming background. *J Clim* 25:3431–3436
- Zuo Z, Yang S, Zhang R, Jiang P, Zhang L, Wang F (2013) Long-term variations of broad-scale Asian summer monsoon circulation and possible causes. *J Clim* 26:8947–8961